Journal of Sol-Gel Science and Technology (2026)117:34
https://doi.org/10.1007/s10971-025-07050-7

ORIGINAL PAPER

Similarities and differences between tannin- and resorcinol-based carbon aerogels: nitrogen-doping, electrical conductivity, and performance in a Zn-based electrochemical cell

Jessica Kröner[1] · Daniela Söllinger[2] · Ann-Kathrin Koopmann[2] · Christoph W. Thurner[3] · Simon Penner[3] · Michael S. Elsaesser[2] · Marina Schwan[1]

Received: 18 July 2025 / Accepted: 18 November 2025

Abstract

Carbon aerogels derived from organic precursors are gaining attention in various applications, especially in energy storage. On one hand, this paper deals with the substitution of phenolic materials by tannin which could be beneficial to both the bioeconomy and the environment due to its low-cost, bio-based, and non-toxic characteristics. On the other hand, the comparative study aims to explore advantages and drawbacks of both aerogels, their electrical conductivity, morphology, performance in an electrochemical cell, and materials costs. The results illustrate that both nitrogen-doped aerogels exhibit pyridinic and pyrrolic functional groups, while doping with melamine leads to higher nitrogen amount about 5 wt.-% compared against ammonia treatment (1–2.5 wt.-%). RF-based carbon aerogels exhibit almost twice the electrical conductivity of tannin-based carbon aerogels. The electrochemical performance of both carbon aerogels in an electrochemical cell is comparable to literature-reported cases. The capacitance of non-doped aerogels was found to be the highest, reaching 239 $F{\cdot}g^{-1}$ at a current density of 0.5 A g^{-1}. Material costs of tannin-based electrodes are slightly lower compared to those based on resorcinol.

Graphical Abstract

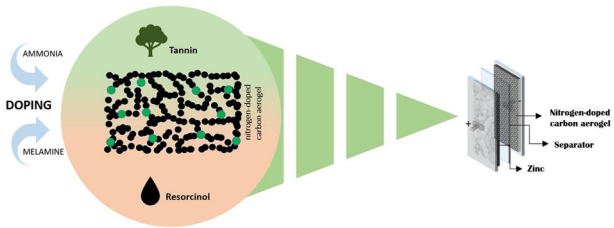

Keywords Porous material · Electrical conductivity · Supercapacitor · High surface area carbon · Micropores · Nitrogen doped carbon

✉ Marina Schwan
Marina.Schwan@dlr.de

[1] Institute for Frontier Materials on Earth and in Space, German Aerospace Center, Cologne, Germany

[2] Chemistry and Physics of Materials, University of Salzburg, Salzburg, Austria

[3] Institute of Physical Chemistry, University of Innsbruck, Innsbruck, Austria

Published online: 05 February 2026

Highlights

- Synthesis of tannin- and resorcinol-based carbon aerogels.
- Thermal activation and nitrogen doping of carbon aerogel.
- Relationship between structural, chemical and physical properties.
- Performance of electrochemical measurements in supercapacitors.
- Costs estimation of aerogel-based electrode materials.

1 Introduction

Carbon aerogels are highly porous solid materials and a huge variety of synthetic pathways were developed in the last 30 years based on the carbonization of organic precursors. This includes classical synthetic systems, such as resorcinol-formaldehyde [1] or tannin-formaldehyde [2–4], and many natural, sustainable organic materials [5]. The open porous network with tunable morphology provides a highly flexible material design to adapt the carbon matrix to different application requirements. The aerogels' characteristics can be varied in terms of mechanical flexibility [6], chemical structure [7–11], electrical conductivity [12], porosity (micropore/mesopore ratio), and density [13].

High inner surface areas and high pore volumes [13] of carbon aerogels lead to broad fields of applications, including catalysis by metal doped carbon aerogels [14] or for the adsorption of gases in foundry applications [15]. Due to their electrically conducting network [16], carbon aerogels are promising candidates for energy storage applications including, but not limited to, supercapacitors [17], lithium-sulfur- [18], rechargeable lithium-based batteries [19], among others [20].

Based on the development of supercapacitors [21], where two principles of storage were claimed: the total capacitance of an electrochemical capacitor consists of the double-layer capacitance and the pseudocapacitance:

- The charge is stored in a Helmholtz double layer, at the interface between an insoluble solid electrode surface and a liquid or solid electrolyte;
- The pseudocapacitance is based on Faradic charge transfer, without chemical reactions with electrodes. Several processes such as intercalation, electrosorption, or redox processes on the surface of the electrodes can induce the charge transfer [22, 23].

Mayer et al. published in 1993 the first electrochemical data on carbon aerogels as an electrode material for supercapacitors [24]. The authors studied the influence of catalyst amount on the capacitance and concluded that the particle size plays a crucial role. The smaller the particle size the higher the capacitance. Small particles connected by smaller contact areas enhanced low contact resistivity leading to a higher performance. Fischer et al. studied the influence of the carbonization temperature on the capacitance and found that the highest capacity was achieved at 800 °C, where a very high micropore volume was formed [25]. The reason for the high capacitance was explained by the existence of pseudocapacitance most likely originating from organic groups on the surface. Several researchers have investigated the role of micro- and mesopores on the capacity. The micropores were found to be important because they participate in the charge storage process. Mesopores in the aerogel's structure also strongly influence the performance of supercapacitors. The best voltammetry characteristics and the highest capacitance were observed with carbon aerogels exhibiting a pore diameter in the range of 3 –13 nm leading to a specific capacitance of 104 F $g^{-1.}$ [26]. Zinc as counter and reference electrode allows the use of aqueous electrolytes, which thereby enhances safety and sustainability compared to commercialized electrochemical cells incorporating organic electrolytes. In addition, the small ionic radius combined with the double charge of Zn-ions, can lead to high volumetric specific capacities [27]. The effect of thermally induced physical activation was studied by several authors. The activation with hot air was found to induce a pseudocapacitance effect, which leads to the improvement of specific capacitance [28]. Among others, metal and nitrogen doping lead to improved electrochemical performance [28–32]. The nitrogen doping was revealed to be an effective technique to increase the electrochemical reactivity of carbon aerogels, as nitrogen provides more active sites for electrochemical reactions on the interface. Braghiroli et al. describe in their study aminated tannin-formaldehyde for supercapacitors [33]. The authors used concentrated ammonia solution for nitrogen-doping and observed outstanding specific capacity compared to non-doped aerogels with higher surface area. They also postulated that the optimal nitrogen amount was about 2–3 wt.% to achieve high capacity. Another study describes the importance of mesopores in the range of 3–13 nm in N-doped carbon aerogels and also a beneficial role of oxygen doping [34]. However, the presence of oxygen can also hinder the diffusion of ions and lead to a decrease in capacity. The authors could achieve 387.6 F g^{-1} at 2 mV s^{-1} [35] with oxygen and nitrogen doped carbon aerogels based on tannin-formaldehyde. Even though, many studies already exist, they describe the activation and doping of

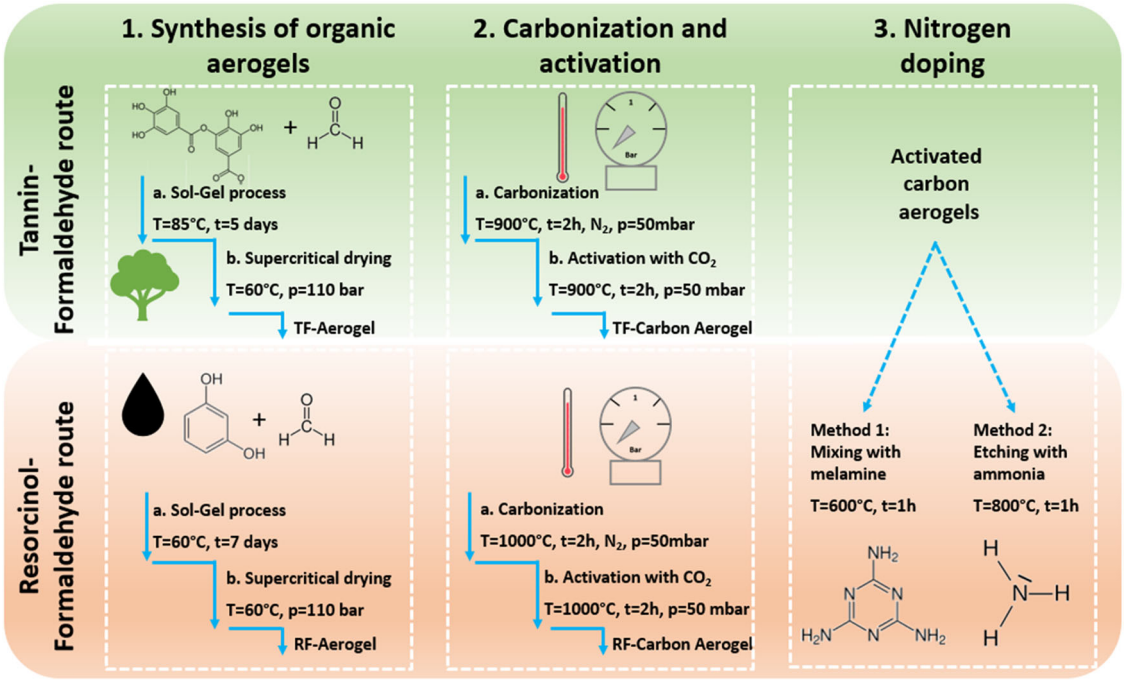

Fig. 1 Schematic representation of the chronological synthesis of aerogels: Sol-gel process, based on either tannin or resorcinol and formaldehyde (1st step), carbonization and physical activation (2nd step), two variants of nitrogen doping (melamine and ammonia route, respectively—3rd step)

only one type of aerogel. In contrast, in our work we summarize the influences of the treatments on both carbon aerogels, tannin and resorcinol based.

Additionally, a large number of surface defects are introduced during doping, so that further improvement of electrical conductivity can be observed. Einert et al. postulated that nitrogen bonding configuration, textural structure, and surface area are critically important parameters for energy-storage applications [36].

In our study, two different kind of carbon aerogels, either made from resorcinol-formaldehyde or tannin-formaldehyde compositions are compared, as depicted in Fig. 1. Furthermore, to the best of our knowledge, we investigated the effectiveness of two different nitrogen doping protocols on both carbon aerogels in one study for the first time. Additionally, for the first time examinations on electrical conductivity of both aerogels complete this study. As a result, our work comprises the influence of thermal activation and nitrogen doping on the microstructure of the carbon aerogel types as well as their impact on the electrochemical performance. The understanding of activation and heteroatom doping is important due to unique microstructure—properties—relationship of carbon aerogels. Even though, RF- and TF-based aerogels have been studied quite extensively in the literature, a comparison between the two is lacking. Our work brings two aerogel types together and shows how different their structures can be with the same treatment parameters. Research in the field of organic and carbon aerogels is advancing to develop more cost-effective and sustainable carbon aerogels from renewable resources, to reduce reliance on fossil fuels and address environmental pollution, and to tailor their structure for enhanced performance in these diverse fields, e.g. energy applications such as batteries, superconductors, fuel cells.

2 Materials and methods

2.1 Synthesis of tannin-formaldehyde (TF) aerogels

Tannin-Formaldehyde aerogels are synthesized in accordance with the study of Amaral-Labat et al. [37]. Tannin (Fintan OP, Silvachimica S.r.l.) (T) was dissolved at room temperature in an aqueous methanol-solution 20 vol.-% (purity ≥99%, Carl Roth) with a mass ratio of 0.1 under stirring at 300 rpm using a cross-magnetic stirring bar. An aqueous solution of formaldehyde (37% w/w, stabilized with 10% methanol, Merck) (F) with a mass ratio T/F of 1.35 was then added to the stirred tannin solution. After 10 min of stirring, the pH value was adjusted to 6 by dropwise addition of 1 M sodium hydroxide (Carl Roth). Stirring at room temperature was continued for 30 min, and the homogeneous solution was poured into sealable polypropylene containers and placed in a furnace at 85 °C (Memmert GmbH, Germany). After 5 days of gelation and aging the wet gel was cooled down to room temperature and transferred into an ethanol bath (technical grade, Th. Geyer)

in order to remove residual reagents and to allow solvent exchange from water to ethanol (necessary for being soluble in supercritical carbon dioxide). The ethanol was refreshed until the water concentration was smaller than 5%. Supercritical drying was carried out with CO_2 (purity, ≥99.995%, Praxair) in an autoclave of 60 L volume (Eurotechnica, Germany) at 60 °C and 115 bars for 21 h. The degassing rate was adjusted to 0.2 bar min^{-1}.

2.2 Synthesis of resorcinol-formaldehyde (RF) aerogels

Resorcinol (R) (98%, Aldrich) was dissolved at room temperature in deionized water (W) with a molar ratio of 0.024 under stirring at 150 rpm using a cross-magnetic stirring bar. An aqueous solution of formaldehyde 23% and 5% w/w stabilized with 1% methanol (F) (R/F 0.5) (Carl Roth) and sodium carbonate (C) (R/C 200) (Aldrich) was then added to the stirred resorcinol solution. Stirring at room temperature was continued for 30 min, and the homogeneous transparent solution was poured into sealable polypropylene containers and placed in an oven at 60 °C (Memmert GmbH, Germany). After 7 days of gelation and aging, the wet gel was cooled down to room temperature and transferred into an acetone bath (pure, technical grade, Th. Geyer) to remove residual reagents and to exchange water by acetone. Acetone was refreshed six times within 3 days until the water content was less than 5%. The supercritical drying was carried out with CO_2 (purity, ≥99.995%, Praxair) in an autoclave of 60 L volume (Eurotechnica, Germany) at 60 °C and 110 bars for about 21 h. The degassing rate was adjusted to 0.2 bar min^{-1}.

2.3 Carbonization and activation

The carbonization was carried out in an electric furnace (KS-3-80-Vac-Sonder, Linn High Therm, Germany) using nitrogen (purity ≥99.999%, Linde). The aerogels were placed in the furnace, purged three times with nitrogen, and heated to the carbonization temperature of 900 °C for TF aerogels and 1000 °C for RF aerogels. The rate was adjusted to 5 K min^{-1}, and the pressure was adjusted to 50 mbar. The temperature was held for 2 h. Subsequently, the activation was performed using CO_2 for 2 h at 900 °C for TF aerogels and 1000 °C for RF aerogels. After carbonization and activation, the aerogels were cooled down to room temperature under a flow of nitrogen.

2.4 Nitrogen doping

For nitrogen doping, two methods were investigated. In the first method, melamine (M) (99%, Alfa Aesar) was used as the nitrogen source. The activated carbon aerogels were mixed with melamine in a mass ratio of 1:1 in a shaker mill (MM400 Retsch, Germany) for 30 s at 30 Hz. Subsequently, the mixtures were thermally treated at 600 °C under nitrogen atmosphere for 1 h. In the second method, the activated carbon aerogels were thermally treated at 800 °C for 1 h under ammonia atmosphere (99.98% NH_3 N38 B10L, Air Liquide) with a flow rate of 0.1 L min^{-1}.

Sample labeling is as follow:

RF-CA: carbon aerogel from resorcinol-formaldehyde.
TF-CA: carbon aerogel from tannin-formaldehyde.
RF-CA_a: activated carbon aerogel from resorcinol-formaldehyde.
TF-CA_a: activated carbon aerogel from tannin-formaldehyde.
RF-$CA_{a,NH3}$: activated carbon aerogel from resorcinol-formaldehyde doped under ammonia atmosphere.
TF-$CA_{a,NH3}$: activated carbon aerogel from tannin-formaldehyde doped under ammonia atmosphere.
RF-$CA_{a,M}$: activated carbon aerogel from resorcinol-formaldehyde doped with melamine.
TF-$CA_{a,M}$: activated carbon aerogel from tannin-formaldehyde doped with melamine.

2.5 Materials characterization

The electrical conductivity of the powdered aerogel samples was investigated using a resistivity measuring system Loresta GX (Mitsubishi Chemical Europe). This system is based on the 4-pin measuring method of surface resistivity at constant pressure. For physisorption experiments the samples were degassed for 12 h at 200 °C and 0.1–0.5 mbar (SmartVacPrep, Micromeritics, Germany). Nitrogen adsorption-desorption isotherms were recorded at 77 K with a 3Flex-apparatus from Micromeritics (Germany). Specific surface areas and pore size distributions were calculated by two-dimensional non-local density functional theory assuming heterogeneous surfaces (HS-2D-NLDFT).

The aerogels' nano-morphologies were analyzed with a JEOL JEM F200 transmission electron microscope (TEM) using an accelerating voltage of 200 kV. The instrument is equipped with a cold field-emission source and a TVIPS F216 2k by 2k CMOS camera. For specimen preparation, the dry powders were placed on lacey carbon films deposited on a Cu grid. Thermogravimetric analysis was performed on a NETZSCH STA 449 F3 Jupiter device in the range of 20 –1000 °C (argon or synthetic air atmosphere).

A Thermo Scientific DXR2 Raman microscope, equipped with a confocal microscope BX41 (Olympus Corp.), was used to collect Raman spectra in the spectral range between 100 cm^{-1} and 3500 cm^{-1} with a 532 nm laser excitation wavelength and a laser power of 4 mW on the sample. A 10× objective (numerical aperture of 0.25),

delivering a laser spot diameter of approximately 2.1 µm was employed. Therefore, a laser intensity on the sample of about 1.2 mW µm^{-2} is obtained. The full range grating with 900 lines mm-1 together with a 50 µm pinhole-like entrance slit to the spectrometer yielded a spectral resolution (equivalent to the full width half maximum of the instrumental line width) of about 1 cm^{-1}.

The combustion elemental (CHNS) analysis was done with an EA300 from EuroVector®. For the combustion analysis the compounds were brayed with vanadium (V) oxide and burned at 1000 °C with subsequent gas chromatography detection.

Surface chemical analysis was carried out in a customized UHV system designed for in situ X-ray photoelectron spectroscopy (XPS) manufactured by SPECS, Berlin. The UHV chamber comprises of a µFOCUS 600 monochromatic small spot (100 × 300 µm^2) Al K_α X-ray source, a hemispherical energy analyzer (PHOBIOS 150 NAP) in vertical configuration and a µ-metal analyzing chamber, shielding the system from external magnetic fields. To investigate polycrystalline samples, a pressed pellet covering a stainless-steel grid as a stabilizer was fixed on a sample-holder by mounting the pellet via a front plate. The excited photo-electrons were collected by a 300 µm nozzle directly from the sample's frontside surface via an 8 mm opening in the front plate. Details of the apparatus can be found in reference, while the sample preparation is based on reference [38] and [39]. Qualitative analysis was based on the O 1 s, C 1 s and Ni 1 s high-resolution spectra. Chemical shifts were calibrated to the carbon component at 285.0 eV [40].

2.6 Electrode preparation and cell setup (in Zn half-cells)

90 wt.% of the active material (90 mg) and 5 wt.% carbon black (5 mg) were ground for 10 min in a mortar. In parallel, 5 wt.% PVDF (5 mg) was dissolved in 3 ml Tetrahydrofuran (THF)/Toluol (2:1, volume ratio) and added to the compounds. The compounds were further ground until a honey-like, viscous slurry was obtained. Afterwards, the slurry was drop casted on a stainless-steel current collector with a maximum active mass between 0.9 mg and 1.6 mg followed by a drying step for at least 3 h at 90 °C in a vacuum furnace. Whatman glass fibers (grade GF/D) were used as the separator and Zn was used as both the counter and reference electrode to establish Zn half-cells. As electrolyte for the electrochemical measurements 2 M $ZnSO_4$ in water was prepared by dissolving the $ZnSO_4$ salt in water for 10 min during stirring under ambient conditions. Galvanostatic measurements were carried out on an eight-channel Astrol BAT-SMALL potentiostat. Specific capacities based on the mass load of the active material were determined by galvanostatic discharge/charge cycling with a constant current. All galvanostatic measurements were carried out in the voltage range of 0.0 V–1.9 V vs. Zn/Zn^{2+} at current densities between 0.5 A g^{-1} and 10 A g^{-1} started with an open circuit voltage of 4 h. For long-term stability measurements a current density of 1 A g^{-1} was used for over 1000 cycles. Cyclovoltammetric (CV) measurements were carried out after C-rate measurements in the voltage range of 0.0 V–1.9 V vs. Zn/Zn^{2+} with a scan rate of 1 mV·s^{-1}. All measurements were performed at ambient conditions.

The specific capacitance was calculated from discharge/charge measurements according to Eq.(1) [41]:

$$[F * g^{-1}] = \frac{I[A] * \Delta t[s]}{m_{EAM}[g] * \Delta U[V]} \quad (1)$$

The energy density was calculated from the first discharge cycle after the initial cycle according to Eq.(2):

$$W[Wh * kg^{-1}] = \frac{1}{m_{EAM}[g]} \int_{t1}^{t2} I(t)[A] * U(t)[V] dt \quad (2)$$

In this context, m_{EAM} refers to the active mass of the cathode material for all measurements.

3 Results and discussion

In this section, the effect of activation with CO_2 is discussed and is followed by a discussion on nitrogen doping. Results of electrochemical performance and economic considerations conclude the section.

In general, both aerogels were synthesized via a sol-gel process. After sol-gel processing and aging in an oven the samples were washed with acetone and dried with supercritical carbon dioxide. Dried aerogels were first carbonized and in a second step activated with CO_2. In order to compare the properties of carbonized and activated aerogels, their microstructure, electrical conductivity, and chemical content were analyzed. The carbonization temperature for both aerogels was chosen based on the literature. For tannin-based aerogel it is typically 900 °C; for RF aerogels, 1000 °C. The vacuum, duration, and gas were identical. Thus, differences in properties, especially in density, electrical conductivity, and microstructure are expected. The activation with CO_2 was carried out under the same conditions for both carbon aerogels.

In the next step activated carbon aerogels were doped with nitrogen via two different methods. Doping with solid melamine took place at 600 °C and the ammonia doping was carried out at 800 °C. Due to the several differences in doping process, such as solid melamine vs. gaseous ammonia and different temperatures, it can be anticipated that the effect of doping will be also different. That would

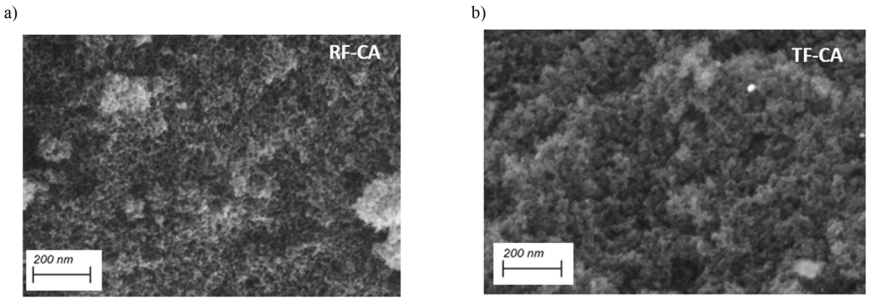

Fig. 2 SEM images of carbon aerogels. **a** Microstructure of non-activated RF-CA consists of small particles and pores of similar size. **b** Microstructure of non-activated TF-CA showing dense structure and slightly larger particles compared to RF-CA

result in changes in the microstructure and electrical conductivity, as well as different nitrogen content.

3.1 Preparation of organic aerogels and their carbon variants

For carbon aerogel preparation, two synthetic routes, depicted in Fig. 1 were employed with regard to the usage of sustainable precursors vs. petrochemical ones as well as subsequent, suitable potential for physical activation and nitrogen doping. In a first step, the aerogel network formation was promoted by a sol-gel process of either tannin-formaldehyde (green variant) or resorcinol-formaldehyde (as classical route for comparison). After gelation and aging at elevated temperatures the build-up of the filigree, nanostructured and highly porous network is completed. TF and RF aerogels were obtained upon supercritical drying with carbon dioxide to avoid severe collapse and shrinkage. Carbonization took place in a tube furnace under an inert atmosphere with the associated release of oxygen and hydrogen containing fragments leading to microporous carbon aerogels. In both cases, stable monolithic sample bodies were obtained. Figure 2 depicts SEM micrographs of their typical, three-dimensional morphology consisting of interconnected nanometer small beads, with the TF aerogel structure being slightly rougher than the RF variant. High-resolution TEM images (Supporting Information, Figure S1*) show smaller particles in RF-CA structure compared to* TF-CA network.

3.2 Effect of physical activation with CO_2 on the aerogel microstructure

Since micropores contribute to the charge storage process in supercapacitors, it is expected that activation of the aerogels lead to higher capacities [42]. Thus, subsequent pore tuning (increase of micropore content, increase of specific surface area (SSA) and, controlled adjustment of pore sizes) was realized by physical activation with carbon dioxide. Directly after the carbonization process, the samples were exposed to carbon dioxide atmosphere for 2 h at elevated temperatures. This allows efficient carbon etching in the pores, described by the Boudouard equilibrium. Nitrogen sorption isotherms were recorded before and after CO_2 activation (Fig. 3a) and evaluated by two-dimensional non-local density functional theory assuming heterogeneous surfaces. The results are summarized in Table 1, featuring details about the pore volume and area induced by solely micropores as well as the total pore volume and overall specific surface area. For both types of aerogels (resorcinol- and tannin-based), a similar isotherm shape was observed: the step increase at very low relative pressures indicates the nitrogen uptake via microporosity, while the typical type IV isotherm with H1 hysteresis in the range of 0.8 – 0.95 p/p_0 is a result of capillary condensation phenomenon due to mesoporosity [43]. Interestingly, while the resorcinol-formaldehyde based carbon aerogels (RF-CA) show no significant increase in porosity and SSA after CO_2 treatment, tannin-based aerogels show enhanced microporosity as well as increased SSA of 709 $m^2\ g^{-1}$ and 934 $m^2\ g^{-1}$, respectively. Similar observations were done by other authors. Amaral-Labat et al. described an increase of surface area for TF carbon aerogels of about 82% even after 20 min of CO_2 activation [44]. Rasines et al. observed an increase of specific surface area of RF carbon aerogels after 2 h CO_2 activation of only 32% [45]. It seems the activation with CO_2 has a different impact on the structure. For TF the changes are more drastic compared to RF, where the structure is also changed but not as strongly as for TF. This can be explained the differences in the densities of both aerogels or in the chemical structure (e.g. oxygen content) of both precursors [46]. Further investigations are required to study the influence of CO_2 on the microstructure of aerogels from different precursors. The calculated pore size distributions, depicted in Fig. 3b, show for both aerogel types the existence of micropores with a size of 1 nm but differences in the mesopore size. While the mesopore size for RF-based carbon aerogels is in the range of 7 –15 nm, the tannin-based variants show larger mesopore sizes in the range of 15 –25 nm, presumably caused by the different molecular sizes of the reactants resorcinol and tannin.

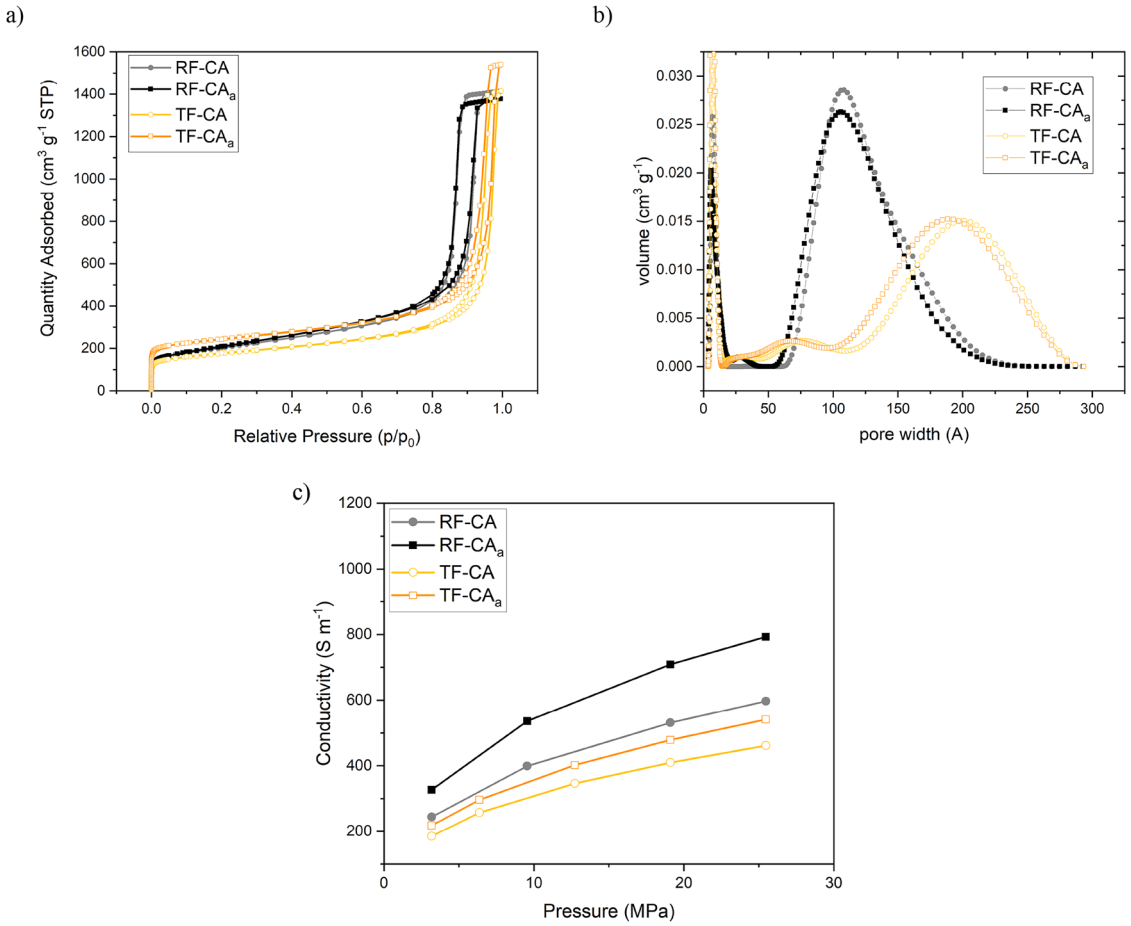

Fig. 3 **a** Nitrogen sorption isotherms, recorded at 77 K, for resorcinol- and tannin- based carbon aerogels before and after activation with carbon dioxide **b** pore size distributions for resorcinol- and tannin-based carbon aerogels before and after activation with carbon dioxide **c** electrical conductivity of powdered carbon aerogels at different pressure

Table 1 Properties of non-activated and activated carbon aerogels

Sample	V_{micro} [cm³ g^{-1}]	A_{micro} [m² g^{-1}]	$V_{sum\ up\ to\ 30\ nm}$ [cm³ g^{-1}]	SSA_{NLDFT} [m² g^{-1}]
RF-CA	0.13	327	2.16	668
RF-CA$_a$	0.13	343	2.11	700
TF-CA	0.16	408	1.77	610
TF-CA$_a$	0.25	709	1.98	934

It is assumed, that the pore characteristics might also influence the aerogel's electrical conductivity. Therefore, the electrical conductivity of activated and non-activated carbon aerogels prepared from RF and TF at different pressures was measured at different pressures (Fig. 3c). With increased pressure, the conductivity arises, due to densification of powder and creating of new pathways for electron transfer. The electrical conductivity of RF-based carbon aerogels is higher compared to TF-based aerogels. A morphological analysis was made by transmission electron micrographs. TEM images (Supporting Information, Fig. S1) show smaller particles of RF-based carbon aerogel and much denser network after activation. Thus, higher contact areas between single particles cause the creation of new pathways for the electron flow. The same trend was observed in a recently published study [47].

Moreover, higher conductivity could be attributed to the carbonization and activation temperature, which was lower for TF-based aerogels [48]. This means that the elevated temperature resulted in different microstructures for the aerogels under the experimental conditions applied, although some rearrangements in the porous structure resulting from thermal annealing may also have occurred, as observed in a previous study for carbon dioxide treatment of lignite chars [49]. Since the activation with CO_2 is based on the Boudouard reaction, the changes in the microstructure during activation strongly depend on the applied temperature. At high temperatures, the forward reaction becomes favored, leading to significant changes in the structure [50]. For both RF- and TF-based carbon aerogels, an increase of the electrical conductivity can be observed after activation.

Table 2 Properties of activated and doped aerogels

Sample name/ Doping method	V_{micro} [$cm^3\ g^{-1}$]	A_{micro} [$m^2\ g^{-1}$]	$V_{cum\ up\ to\ 30\ nm}$ [$cm^3\ g^{-1}$]	SSA_{NLDFT} [$m^2\ g^{-1}$]	N-content [wt.-%]
RF-CA_a	0.13	343	2.11	700	–
RF-$CA_{a,NH3}$	0.18	341	2.09	681	1.37
RF-$CA_{a,M}$	0.14	352	2.00	680	3.63
TF-CA_a	0.25	709	1.98	934	–
TF-$CA_{a,\ NH3}$	0.22	585	1.67	794	2.54
TF-$CA_{a,M}$	0.14	389	1.51	563	4.83

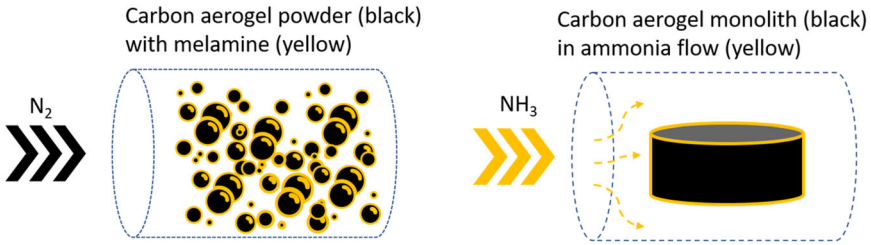

Fig. 4 Schematic visualization of doping methods used in the study. Left: N-doping with solid melamine on powdered carbon aerogels; Right: N-doping in ammonia atmosphere on monolithic aerogels

3.3 Comparison and discussion on different nitrogen doping techniques and its effect on chemical structure

Nitrogen doping of activated carbon aerogels (RF and TF) was realized by two methods: For the first route, the monolithic carbon samples were placed in a tube furnace and treated with ammonia gas at 800 °C for 1 h. After cooling down in an argon atmosphere, visually unchanged samples were obtained. For the second route, solid melamine was added to the powdered activated carbon aerogel powder and intensively mixed, followed by heating to 600 °C under an inert atmosphere. To monitor the effect of nitrogen content, elemental analysis was performed and showed for both variants significant nitrogen content. While doping with ammonia resulted in N-contents of 1 wt.%–2.5 wt.%, the nitrogen content was increased by the melamine method up to nearly 5 wt.% (Table 2). Doping with melamine resulted in almost double the amount of N compared to ammonia treatment. The reason for this could be a surface effect caused by the doping method. While doping with melamine, the aerogel was crushed in a mill together with melamine so that the doping agent is homogeneously distributed in the aerogel powder as shown in Fig. 4 (left). In the case of ammonia treatment, monolithic aerogels were placed in the oven and then doped by the reaction in the NH_3 flow, Fig. 4 (right). One could assume that this method is well suited for external surface doping because the aerogel is placed in the NH_3 flow and is less suitable for doping inside the structure of large monoliths with the applied settings (800 °C for 1 h under ammonia atmosphere with a flow rate of 0.1 L min^{-1}). To reach higher or comparable amounts of nitrogen, either the duration of ammonia treatment should be increased or the NH_3 flow through the furnace should be higher. Nevertheless, the optimal nitrogen amount (about 2–5 wt.%) to achieve high electrochemical capacity [34] was achieved with both methods. Remarkably, the N-content is in general lower for RF than for TF based carbon aerogels. This may be due to the fact that RF carbon aerogels have a lower surface area compared to TF. For melamine doped aerogels, the difference is about 33%. For surface sensitive ammonia doping the difference is much higher (about 85%), which corresponds well with our hypothesis of predominantly external surface N-doping with that method. To sum up we can conclude that doping in ammonia flow is an external surface sensitive method and thus, it is more effective for aerogels with high surface area.

Possible pore variations after nitrogen doping were monitored by nitrogen physisorption measurements. Generally, the isotherm characteristics (Fig. 5a) for TF- and RF-based carbon aerogels did not change upon nitrogen doping. In turn, both features for the presence of micropores and mesopores (step N_2 uptake at low relative pressures and H1 hysteresis) were obtained and the corresponding pore size distribution (Fig. 5b) showed the afore mentioned sizes: 1 nm for micropore size and different mesopore sizes, 7–15 nm for RF-based aerogels and 15 nm–25 nm for TF-based aerogels. Furthermore, a general decrease in pore volume and SSA was obtained upon nitrogen doping. This observation was less distinct for the RF-based aerogels, e.g., decrease of around 20 $m^2\ g^{-1}$ after N incorporation, while for the activated and ammonia doped TF-based aerogel showed a decrease in SSA from 934 $m^2\ g^{-1}$ to 563 $m^2\ g^{-1}$ (Table 2). A similar trend was observed for the micropore-volume and surface area: nearly no decrease for the RF-

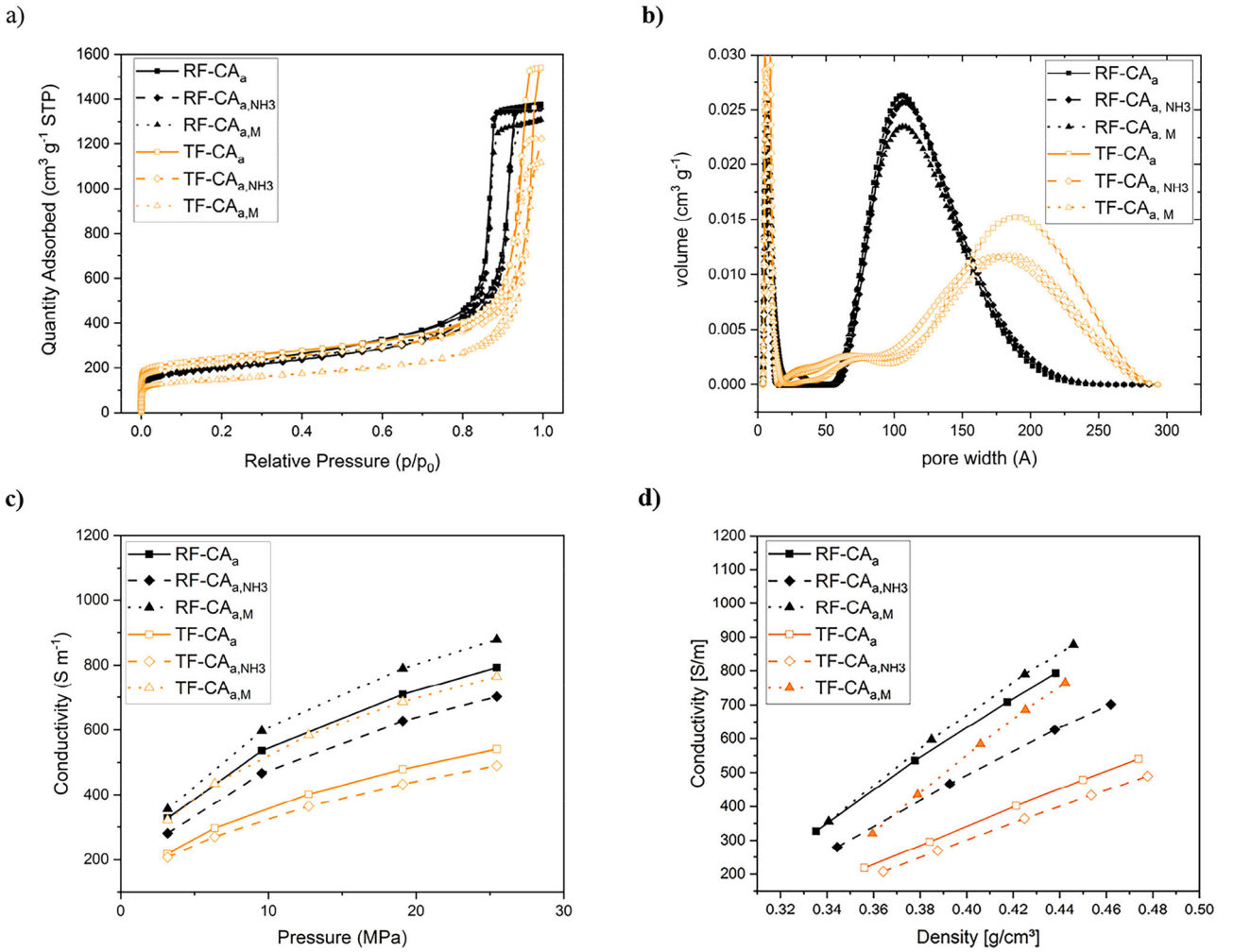

Fig. 5 **a** Nitrogen sorption isotherms, recorded at 77 K, for activated and doped resorcinol-and tannin- based carbon aerogels after activation with CO_2, N doping and melamine doping **b** pore size distributions for activated and doped resorcinol- and tannin- based carbon aerogels. **c** Electrical conductivity of carbon aerogels showing strong effect of doping agent **d** powder density of carbon aerogels

based carbon aerogel, but a decrease in the range of 40% for the TF-based variant. It is noticeable that the reduction in surface area and pore volume is more pronounced in the melamine-doped samples. Liu et al. observed significant changes in the structure after melamine-doping [51]. Melamine creates a smooth sub-structure on the particle surface. This continuous structure can act as a highly conductive layer, causing a significant increase in the electrical conductivity but it can also block the pores.

The effect of the doping agent on the electrical conductivity is visualized in Fig. 5c. Compared to only activated carbon aerogel, doping with melamine increases the conductivity, while doping with ammonia leads to its decrease. The amount of nitrogen after melamine-doping is almost two times higher compared to ammonia-doping, as depicted in Table 2. These results from elemental analysis are in agreement with X-ray photoelectron spectroscopy (XPS) results (Fig. 7). Ayiania et al. have also observed differences in nitrogen content by varying the doping agents [40]. The nitrogen content when using ammonia increases with increased temperature due to reaction of ammonia with carbon only at temperatures above 500 °C, while nitrogen content with melamine doping shows the opposite trend. Nitrogen amount decreases nearly linearly between 350 °C and 700 °C. It can be concluded that the melamine doping was successful and led to increasing conductivity.

The powder densities of the aerogels are depicted in Fig. 5d. The densities are in the range of 0.33–0.37 g cm³. The RF-based aerogels are slightly lighter than TF-based samples. It is expected that due to the higher temperature involved in ammonia treatment and higher densities of NH_3-doped aerogels (Fig. 5d), the electrical conductivity of those aerogels should be higher compared to melamine doped material. However, our measurements show the opposite trend. The melamine doped aerogels exhibit much higher conductivities for both aerogels. Celzard et al. have

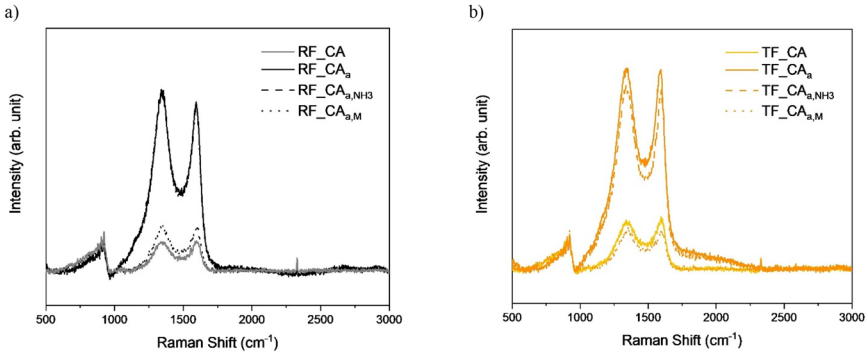

Fig. 6 Raman spectra of pristine **a** RF-based and **b** TF-based carbon aerogels before and after CO_2 activation and nitrogen doping

Table 3 Peak area ratios of the D- and G-bands (A_D/A_G) of aerogels

Sample	Band	Position [cm^{-1}]	FWHM [cm^{-1}]	A_D/A_G
RF_CA	D-band	1348	129	2.3
	G-band	1601	68	
RF_CA$_a$	D-band	1346	121	2.1
	G-band	1597	68	
RF_CA$_{a,NH3}$	D-band	1345	119	2.1
	G-band	1597	65	
RF_CA$_{a,M}$	D-band	1351	118	2.0
	G-band	1601	71	
TF_CA	D-band	1348	146	2.6
	G-band	1599	68	
TF_CA$_a$	D-band	1341	135	2.8
	G-band	1591	66	
TF_CA$_{a,NH3}$	D-band	1345	134	2.6
	G-band	1597	65	
TF_CA$_{a,M}$	D-band	1358	128	2.0
	G-band	1602	69	

investigated the effect of particles morphology on the electrical conductivity of carbonaceous powders [52]. They emphasized the influence of particle shape, size and the way the grains of powder are packed. Similar observations on the influence of particle shape on electrical conductivity were published recently [47]. As discussed earlier, formation of a layer-like structure during melamine doping can also lead to an increase in electrical conductivity. The layer serves as an additional path for electron transfer. Deeper insights into the morphology of powdered carbon aerogels is needed and is a goal of upcoming studies. Furthermore, the carbonization temperature is probably the decisive factor influencing the conductivity.

The chemical nature of the synthesized RF and TF carbon aerogels was investigated using Raman spectroscopy. The obtained Raman spectra (Fig. 6) show the characteristic D-band and G-band at 1348 cm^{-1} and 1598 cm^{-1}, respectively. The D- and G-band are associated with the sp^2-hybridized disordered carbon (A_{1g} in-plane breathing vibration mode) and ordered graphite (E_{2g} in plane vibration mode), respectively. An increase in D-band intensity is associated with a more disordered carbon structure. Furthermore, the peak area ratio of the D- and G-band (A_D/A_G) indicates the relative graphitization degree of a carbon material [53]. Similar to other resorcinol-based [54] and tannin-based carbons [41], peak area ratios A_D/A_G of 2.1 and 2.5 are obtained, respectively. This is consistent with incomplete crystallinity as the majority of the synthesized carbon material has an amorphous nature. Moreover, the high degree of disorder of the doped carbon material is also revealed by the broadening of the D- and G-band. Thus, these bands are cumulatively fitted by deconvolution into the bands D*, D, D**, G, and D$'$ in accordance to Kaniyoor and Ramaprabhu [55] (Supporting Information, Fig. S2).

Table 3 summarizes the peak area ratios of the D- and G-band of the carbon aerogels. It can be seen that A_D/A_G decreases slightly for doped aerogels, which indicates a low degree of crystallinity. For activated carbon aerogels, no clear trend can be seen. For TF-based aerogels, more defects seem to be introduced into the structure, while RF-based aerogels show an increase of graphitization degree probably caused by higher carbonization and activation temperature, as discussed earlier.

For carbon aerogels, XPS provides valuable insights into the elemental composition and chemical state, especially with regard to functional groups present on the surface, With respect to the C 1 s spectra, typical asymmetric shapes for nitrogenated char samples, independent of the specific preparation routine, were observed [40]. The main C 1 s peak was found at a binding energy (BE) of ≈284,6 eV (Fig. 7a). No pronounced chemical shift as a function of the preparation routine was recorded. Ayiania et al. infer that this peak is a result of the loss of oxygen and nitrogen functional groups and the condensation of aromatic structures [40]. A clear dependence on the synthesis routine was detected in the N 1 s spectra. As the RF-CA$_a$ and TF-CA$_a$ samples did not contain nitrogen, no N 1 s peak appears. The nitrogen-doped samples show a similar N 1 s peak shape and BE but different in intensity which suggests that a different amount of similar N-functionalities are present at the surface. In essence, a main peak at ≈398.3 eV

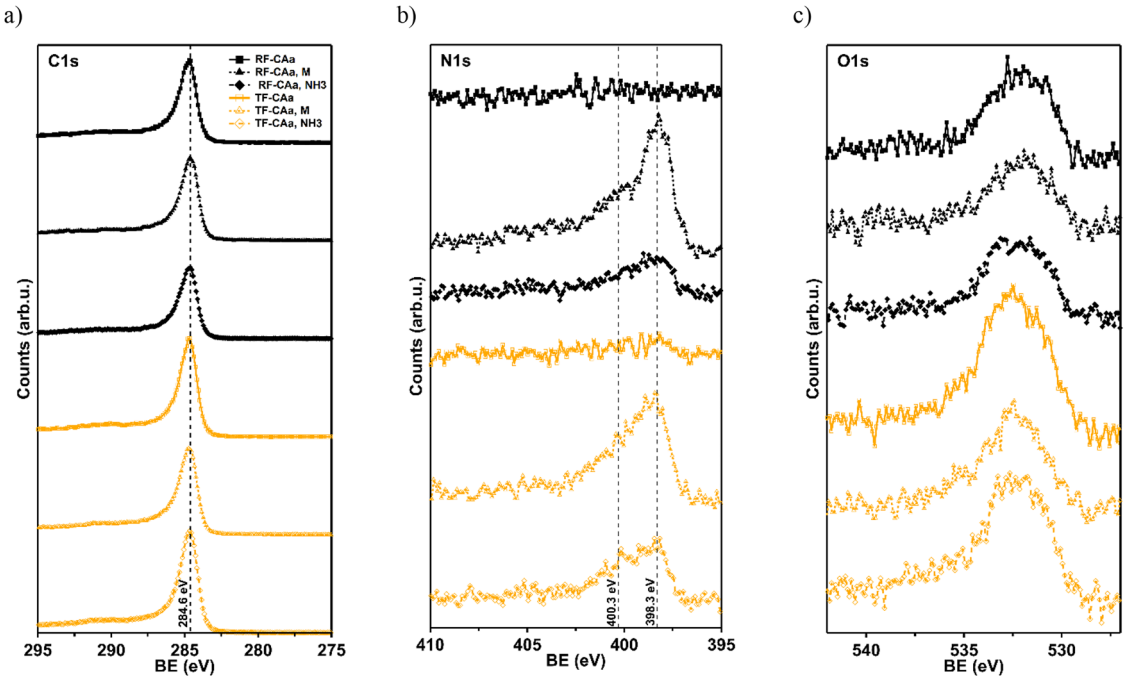

Fig. 7 X-ray photoelectron spectra of solely activated and nitrogen doped carbon aerogels (RF- and TF-based): **a** C 1 s region, **b** N 1 s region and **c** O 1 s region

accompanied by a pronounced shoulder at ≈400.3 eV is detected. According to reference [40] these BEs are associated with pyrrolic and pyridinic functional groups, respectively. The comparison of the relative intensities of both peaks indicates that treatment by ammonia balances the amount of pyrrolic and pyridinic groups, while the addition of melamine favors the formation of pyrrolic functions. The presence of multiple oxygen states results in a broad O 1 s features, which are attributed to hydroxyl or ether groups [40].

Additionally, elemental ratios of activated and doped carbon aerogels were calculated (Table S3 in SI). The results show that addition of melamine leads to a higher amount of N at the surface (5 at.-% in RF-CA and 4 at.-% in TF-CA) compared to ammonia treatment with 2 at.-% of nitrogen, which is in agreement with elemental analysis It has been reported that the amount of surface N is a function of temperature [40], which is reflected in our data. Oxygen is present in all samples, but the data indicate that the RF route causes less surface O (1–2 at.-%) compared to the TF route (2–3 at.-%), being consistent with oxygen levels present in the starting material.

3.4 Electrochemical performance of carbon aerogels

Figure 8 shows C-rate measurements with current densities of 0.5 $A{\cdot}g^{-1}$, 1 $A{\cdot}g^{-1}$, 2 $A{\cdot}g^{-1}$, 5 $A{\cdot}g^{-1}$, 10 $A{\cdot}g^{-1}$, and 0.5 $A{\cdot}g^{-1}$ and cyclovoltammetric measurements of cells containing RF-CA and TF-CA samples as cathode, zinc as counter and reference electrode and 2 M $ZnSO_4$ in water as electrolyte. All cells were first discharged to 0.0 V vs. Zn/Zn^{2+} and afterwards charged to 1.9 V vs. Zn/Zn^{2+} with the above-mentioned current densities each for 5 cycles.

Figure 8a, b shows that all modifications have similar specific capacities and capacitances. Although the RF-CA samples have a higher conductivity compared to the TF-CA, they also have smaller surface areas (Table 2).

Since both criteria, high surface areas as well as the electrical conductivity, have an influence on the electrochemical properties, it is assumed that the effects cancel each other out and therefore no significant differences between the RF-CA samples and the TF-CA samples are visible.

Figure 8c shows the cyclovoltammetric measurements, which have a typical shape for electric double layer behavior. The curve during the discharging and charging process, as well as the total area, is again similar for all RF-CA and TF-CA samples.

Only the $RF\text{-}CA_a$ sample appears to show an increase in the electrochemical measurements compared to their modifications. This can also be seen by the corresponding charge-discharge curves, the calculation of the energy density for low current densities and the Ragone plot in the Supporting Information in Figs. S5, S6 and Table S4, as well as Fig. S7, respectively. In this case, it is possible that further aspects, *e.g.*, different parameters during the synthesis for $RF\text{-}CA_{a,NH3}$ and $RF\text{-}CA_{a,M}$ have an influence on the electrochemical properties compared to the $RF\text{-}CA_a$ sample.

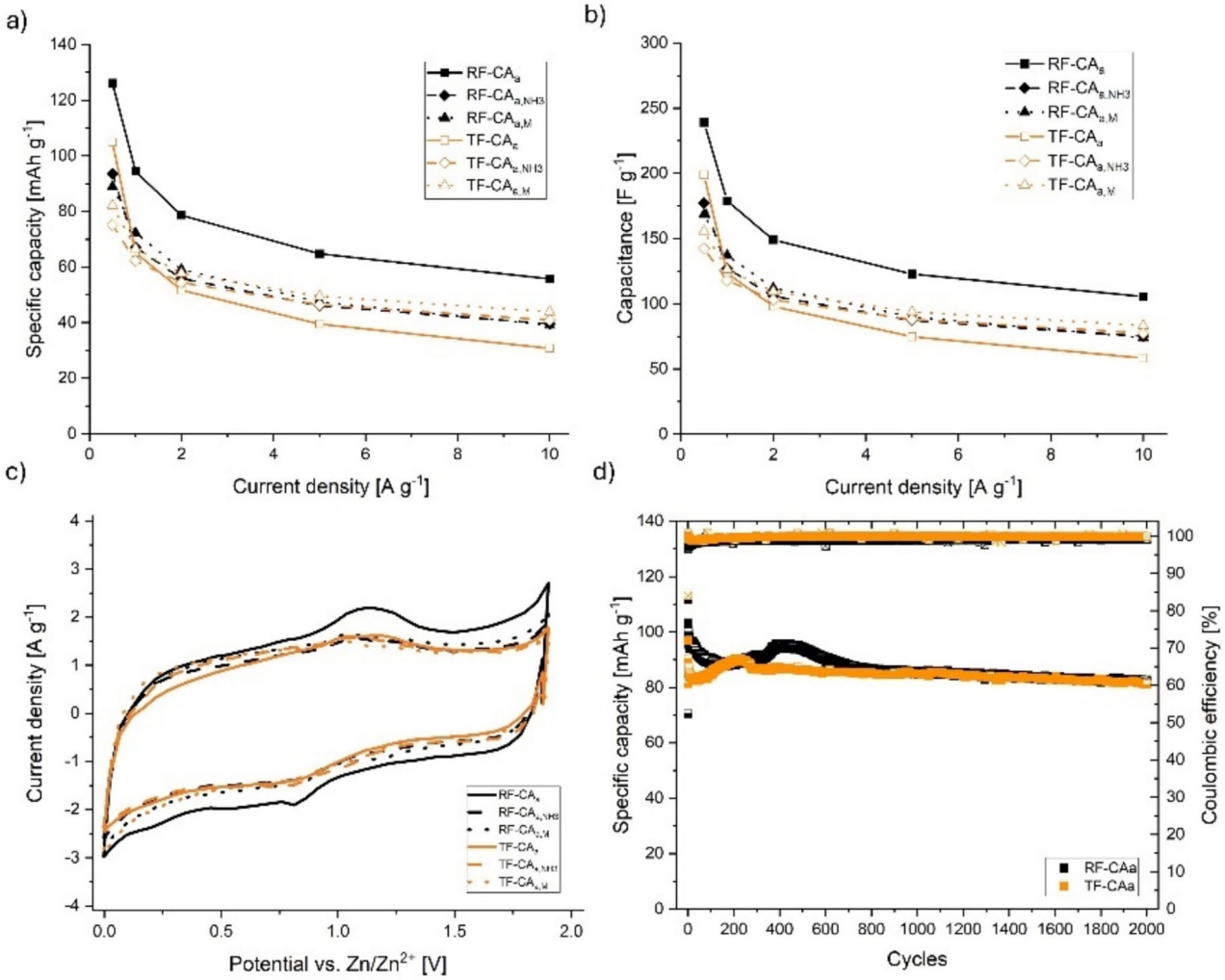

Fig. 8 Electrochemical performance of carbon aerogels in the potential range 0.0–1.9 V vs. Zn/Zn^{2+}—**a** and **b** C-rate measurements to obtain the specific capacity ($mAh{\cdot}g^{-1}$) and the capacitance ($F{\cdot}g^{-1}$) at current densities of 0.5 $A{\cdot}g^{-1}$, 1 $A{\cdot}g^{-1}$, 2 $A{\cdot}g^{-1}$, 5 $A{\cdot}g^{-1}$ and 10 $A{\cdot}g^{-1}$, **c** CV-measurements at a sweep rate of 1 $mV{\cdot}s^{-1}$. The CV-measurements were carried out after the C-rate measurements and **d** long-term stability measurements of $RF\text{-}CA_a$ and $TF\text{-}CA_a$ at a current density of 1 $A{\cdot}g^{-1}$

However, the difference of the specific capacity is reduced for higher current densities or long-term stability measurements (Fig. 8a, b, d). Furthermore, no differences in the electrochemical properties of $TF\text{-}CA_a$ compared to $TF\text{-}CA_{a,NH3}$ and $TF\text{-}CA_{a,M}$ are visible, assuming that doping with N_2 does not lead to significant changes in the electrochemical properties. Even though XPS results show that pyridinic and pyrrolic nitrogen were incorporated, the effects of doping are not visible in the capacitance. In contrast, the results from Lee et al. clearly indicated the significance of contributions of the pyridine and pyrrole functional groups to the supercapacitive properties [56]. In the study, higher capacitance for materials with pyrrolic groups compared with pyridinic groups is confirmed. However, they also mentioned that the surface area as well as the electrical conductivity have a significant effect on the Coulombic interactions and thus the capacitance. As a result, they evaluated and calculated the specific surface area (SSA) using the BET method, confirming that the SSA of the investigated samples are comparable. Furthermore, the capacitance of their samples, increased with higher electrical conductivity [57, 58]. In our study, the electrical conductivity as well as the SSA are different within the samples. TF-samples have lower electrical conductivities than RF-samples (see Fig. 5c) while doped samples show lower SSAs compared to undoped samples (see Table 2). In addition, the N-content shows values between 0 and 4.83 wt.% (see Table 2). Overall, our measurements show that the lower capacitance of ammonia doped aerogels compared to previous studies is attributed to a combination of electrical conductivity [56], low SSA [59] and nitrogen content [60] as all these parameters have a significant impact on the capacitance as presented in previous studies. Nevertheless, the capacitance of 142–239 F g^{-1} at 0.5 A g^{-1}

Table 4 Electrochemical performance of different carbon aerogels

Literature	Carbon Material / Synthesis	Electrochemical Performance
Fischer et al. [25]	Resorcinol formaldehyde- based carbon aerogels	Supercapacitor 46 F cm^{-3}
Braghiroli et al. [34]	Tannin based carbons (N-doped) Hydrothermal synthesis	Supercapacitor 320 F g^{-1} at 2 mV s^{-1}
Sam et al. [35]	Biomass-derived carbon aerogels (N-doped)	Supercapacitor 388 F g^{-1} at 2 mV s^{-1}
Koopmann et al. [41]	Tannin-5-HMF spherogels Sol-gel method	Zinc hybrid supercapacitor 265 F g^{-1} at 0.5 A g^{-1}
Park et al. [17]	Resorcinol formaldehyde- based carbon aerogels Sol-gel method	Supercapacitor 21.8 F·g^{-1} at 2 A·g^{-1}
This work (2025)	Resorcinol and Tannin based carbon aerogels (N-doped)	Zinc based electrochemical cell 239 F g^{-1} at 0.5 A g^{-1}

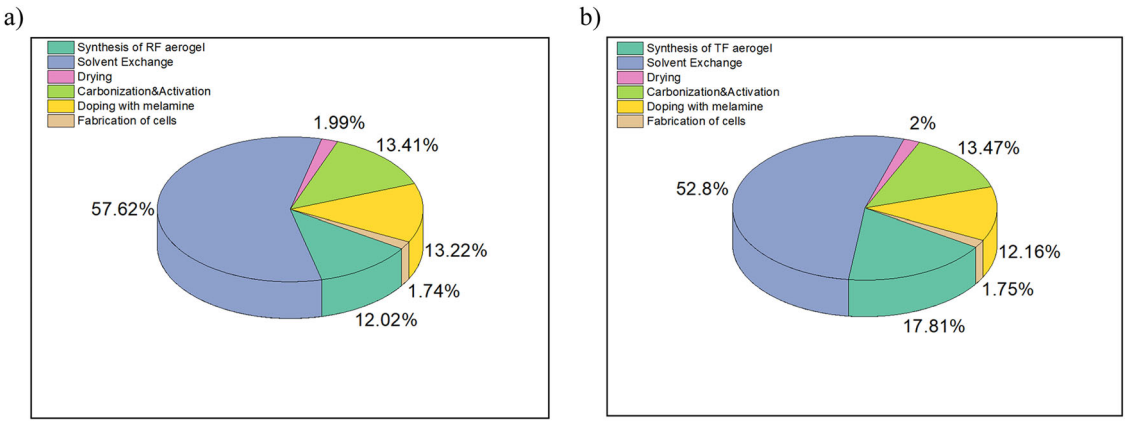

Fig. 9 Material prices for aerogel-based electrodes: **a** 154 €$_{(100g)}$ RF-$CA_{a,M}$ and **b** 144 €$_{(100g)}$ TF-$CA_{a,M}$

measured for our samples show that they are still comparable to other studies (Table 4) and, in addition, are more cost-efficient and sustainable due to the use of Zn as counter electrode and a 2 M $ZnSO_4$ aqueous electrolyte [61]. In this context, RF- and TF-based carbon aerogels offer a more sustainable, safer, and—in some cases—cost-efficient alternative to supercapacitors, which contain critical materials such as Co or Li [57, 58].

To conclude, in our study, against our expectations, the positive effect of the activation process on surface area was canceled with subsequent doping, where we observe a decrease of surface area and at the same time successful incorporation of nitrogen.

3.5 Estimated materials costs for electrode materials

The estimated costs for aerogel-based electrode material are depicted below (Fig. 9). The material costs are essentially made up of 6 categories: synthesis (precursors, formaldehyde, sodium carbonate), solvent exchange (ethanol or acetone), drying in supercritical carbon dioxide (carbon dioxide), carbonization (nitrogen, carbon dioxide), doping with melamine, and cell fabrication.

The most expensive step is solvent exchange due to the high costs of solvents. Based on the literature, TF aerogels are usually washed with ethanol and RF aerogels with acetone to assure low shrinkage [62] [2]. It is followed by raw material costs (tannin, resorcinol, formaldehyde, and sodium carbonate) costs for synthesis. Carbonization and activation as well as doping with melamine account for approximately 12-13% of total costs. Since doping with ammonia was not successful, it is not included in this cost calculation. In general, RF-based electrodes are about 7% more expensive than TF-based electrodes. Higher sustainability of tannin should also be considered, since it is a natural material. We would like to point out only materials costs are listed in that calculation. The energy consumption being a significant part of production costs is not considered in our study. Processes such as supercritical drying, carbonization and thermal treatment are very time and energy consuming steps in the synthesis of aerogels but they are quite similar for both aerogels. In case of TF aerogels, the carbonization took place at 900 °C compared to RF, which was carbonized at 1000 °C. All the other steps were carried out under the same conditions.

Upscaling the production of carbon aerogels involves navigating various technical and economic challenges. While advancements in technology and increased demand may lead to cost reductions in the future, the current production of carbon aerogels remains relatively expensive compared to traditional materials. Upscaling to an industrial scale is recommended not only for economic but also for environmental benefits. Kara et al. have shown substantially reduced environmental impacts from bench to pilot scale

[63]. Continued research and innovation are essential for making these materials more accessible and cost-effective for widespread applications.

4 Conclusions

In this work, we demonstrated the synthesis of resorcinol- and tannin-based carbon aerogels with activation process and nitrogen doping and demonstrated its application for supercapacitor electrodes. It is concluded that the activation and doping interfere with the microstructure of carbon aerogels distinctively. In general, RF-based carbon aerogels are predominantly microporous and exhibit higher electrical conductivities. In both cases, RF and TF aerogels exhibit lower surface area and pore volume after N-doping. In contrast, TF-based aerogels have slightly lower specific surface areas and lower electrical conductivities. XPS results confirm that both doping techniques are suitable to synthesize nitrogen-doped carbon aerogels. However, doping with melamine appears to be more successful in terms of the total nitrogen content at the surface, while an ammonia treatment of monolithic aerogels was shown to be more suitable for doping of external surface area. Nonetheless, the electrochemical analysis shows that the nitrogen doping of RF aerogels and TF aerogels does not lead to desired changes in the electrochemical properties. RF-CAa samples (without any further modifications) exhibit the most promising electrochemical performance. However, the effect of N-doping may become more pronounced at higher current densities (5 and 10 $A \cdot g^{-1}$) as indicated in GDCs (see Figure S5). This behavior - in addition to the correlation of N-content and surface area of the TF- and RF-gels - should be studied in more detail in a follow-up study. Nevertheless, the electrochemical performances of the synthesized aerogels in terms of the capacitance are comparable with previous studies and show, in addition, a higher sustainability and lower costs.

Data availability

The original data are available from the corresponding author upon reasonable request.

Supplementary information The online version contains supplementary material available at https://doi.org/10.1007/s10971-025-07050-7.

Acknowledgements We acknowledge Rebekka Probst (DLR) for SEM images and Salihovic Miralem for TEM images. Valerie Werner and Simone Pokrant are greatly thanked for ammonia furnace treatments.

Author contributions Conceptualization: JK and ME; methodology: JK, DS, AK, CWT, SP; validation: ME; writing—original draft preparation: ME, JK, DS, AK, CWT, SP; writing—review and editing: EM, JK, and SM; funding acquisition: JK. All authors have read and agreed to the published version of the manuscript.

Funding This research was funded by CostAction (COST EU), grant number CA18125-47459. TEM measurements were carried 492 out on a JEOL JEM F200 TEM, funded by the FFG (grant number 37120633). Open Access funding enabled and organized by Projekt DEAL.

Compliance with ethical standards

Conflict of interest The authors declare no competing interests.

Publisher's note Springer Nature remains neutral with regard to jurisdictional claims in published maps and institutional affiliations.

References

1. Pekala RW (1991) Melamine-formaldehyde aerogels, in, Google Patents, USA.
2. Braghiroli FL, Amaral-Labat G, Boss AFN, Lacoste C, Pizzi A (2019) Tannin gels and their carbon derivatives: A review. Biomolecules 9:587.
3. Szczurek A, Amaral-Labat G, Fierro V, Pizzi A, Celzard A (2011) The use of tannin to prepare carbon gels. Part II. Carbon cryogels, Carbon 49:2785–2794.
4. Szczurek A, Amaral-Labat G, Fierro V, Pizzi A, Masson E, Celzard A (2011) The use of tannin to prepare carbon gels. Part I: Carbon aerogels. Carbon 49:2773–2784.
5. Pekala RW (1998) Organic carbon aerogels from the sol-gel polymerization of phenolic-furfural mixtures, in, Google Patents, USA.
6. Schwan M, Ratke L (2016) Flexible carbon aerogels. J Carbon Res 2:22.
7. Chi C, Liu Z, Lu X, Meng Y, Huangfu C, Yan Y, Qiu Z, Qi B, Wang G, Pang H, Wei T, Fan Z (2023) Balance of sulfur doping content and conductivity of hard carbon anode for high-performance K-ion storage, Energy Storage. Materials 54:668–679.
8. Kensy C, Härtel P, Maschita J, Dörfler S, Schumm B, Abendroth T, Althues H, Lotsch BV, Kaskel S (2020) Scalable production of nitrogen-doped carbons for multilayer lithium-sulfur battery cells. Carbon 161:190–197.
9. Marumi M, Tang X, Kesava Rao V, Alodhayb AN, Kulkarni MM, Dwivedi PK, Lisi F, Kitahama Y, Xiao T-H, Goda K (2024) A highly simple and controllable nitrogen-doping method for carbon-based surface-enhanced Raman spectroscopy substrates. Mater Adv 5:4764–4771.

10. Mirzaeian M, Abbas Q, Gibson D, Mazur M (2019) Effect of nitrogen doping on the electrochemical performance of resorcinol-formaldehyde based carbon aerogels as electrode material for supercapacitor applications. Energy 173:809–819.
11. Przepiórski J, Skrodzewicz M, Morawski AW (2004) High temperature ammonia treatment of activated carbon for enhancement of CO2 adsorption. Appl Surf Sci 225:235–242.
12. Pekala RW, Farmer JC, Alviso CT, Tran TD, Mayer ST, Miller JM, Dunn B (1998) Carbon aerogels for electrochemical applications. J Non-Crystalline Solids 225:74–80.
13. Shen J, Guan DY (2011) Preparation and Application of Carbon Aerogels, in: AM Aegerter, N Leventis, MM Koebel (Eds.) Aerogels Handbook, Springer New York, New York, NY, pp. 813–831.
14. Guilminot E, Fischer F, Chatenet M, Rigacci A, Berthon-Fabry S, Achard P, Chainet E (2007) Use of cellulose-based carbon aerogels as catalyst support for PEM fuel cell electrodes: Electrochemical characterization. J Power Sources 166:104–111.
15. Ratke L, Milow B (2011) Aerogels for Foundry Applications, in: MA Aegerter, N Leventis, MM Koebel (Eds.) Aerogels Handbook, Springer New York, pp. 763–788.
16. Worsley MA, Pauzauskie PJ, Olson TY, Biener J, Satcher JH, Baumann TF (2010) Synthesis of graphene aerogel with high electrical conductivity. J Am Chem Soc 132:14067–14069.
17. Park DW, Canas NA, Schwan M, Milow B, Ratke L, Friedrich KA (2016) A dual mesopore C-aerogel electrode for a high energy density supercapacitor. Curr Appl Phys 16:658–664.
18. Nojabaee M, Sievert B, Schwan M, Schettler J, Warth F, Wagner N, Milow B, Friedrich KA (2021) Ultramicroporous carbon aerogels encapsulating sulfur as the cathode for lithium–sulfur batteries. J Mater Chem A 9:6508–6519.
19. Balakumar K, Kalaiselvi N (2015) High sulfur loaded carbon aerogel cathode for lithium–sulfur batteries. RSC Adv 5:34008–34018.
20. He T, Zhang Y, Chen Y, Zhang Z, Wang H, Hu Y, Liu M, Pao C-W, Chen J-L, Chang LY, Sun Z, Xiang J, Zhang Y, Chen S (2019) Single iron atoms stabilized by microporous defects of biomass-derived carbon aerogels as high-performance cathode electrocatalysts for aluminum–air batteries. J Mater Chem A 7:20840–20846.
21. Becker H (1954) Low voltage electrolytic capacitor. Patent US2800616A, in, USA.
22. Simon P, Gogotsi Y (2008) Materials for electrochemical capacitors. Nat Mater 7:845.
23. Zhang LL, Zhao XS (2009) Carbon-based materials as supercapacitor electrodes. Chem Soc Rev 38:2520–2531.
24. Mayer S, Pekala R, Kaschmitter J (1993) The aerocapacitor: An electrochemical double-layer energy-storage device. J Electrochem Soc 140:446.
25. Fischer U, Saliger R, Bock V, Petricevic R, Fricke J (1997) Carbon aerogels as electrode material in supercapacitors. J Porous Mater 4:281–285.
26. Li W, Reichenauer G, Fricke J (2002) Carbon aerogels derived from cresol–resorcinol–formaldehyde for supercapacitors. Carbon 40:2955–2959.
27. Mageto T, Bhoyate SD, Mensah-Darkwa K, Kumar A, Gupta RK (2023) Development of high-performance zinc-ion batteries: Issues, mitigation strategies, and perspectives. J Energy Storage 70:108081.
28. Hwang S-W, Hyun S-H (2004) Capacitance control of carbon aerogel electrodes. J Non-Cryst Solids, 347:238–245.
29. Huang K-J, Wang L, Zhang J-Z, Xing K (2015) Synthesis of molybdenum disulfide/carbon aerogel composites for supercapacitors electrode material application. J Electroanal Chem 752:33–40.
30. Moreno-Castilla C, Maldonado-Hódar FJ (2005) Carbon aerogels for catalysis applications: An overview. Carbon 43:455–465.
31. Zapata-Benabithe Z, Carrasco-Marín F, Moreno-Castilla C (2013) Electrochemical performance of Cu-and Ag-doped carbon aerogels. J Materials Chemistry Physics 138:870–876.
32. Zhai Z, Ren B, Xu Y, Wang S, Zhang L, Liu Z (2019) Green and facile fabrication of Cu-doped carbon aerogels from sodium alginate for supercapacitors. J Organic Electronics 70:246–251.
33. Braghiroli FL, Fierro V, Szczurek A, Stein N, Parmentier J, Celzard A (2015) Hydrothermally treated aminated tannin as precursor of N-doped carbon gels for supercapacitors. Carbon 90:63–74.
34. Braghiroli FL, Fierro V, Szczurek A, Stein N, Parmentier J, Celzard A (2015) Electrochemical performances of hydrothermal tannin-based carbons doped with nitrogen. Ind Crops Products 70:332–340.
35. Kobina Sam D, Kobina Sam E, Lv X (2020) Application of Biomass-Derived Nitrogen-Doped Carbon Aerogels in Electrocatalysis and Supercapacitors. ChemElectroChem 7:3695–3712.
36. Einert M, Wessel C, Badaczewski F, Leichtweiß T, Eufinger C, Janek J, Yuan J, Antonietti M, Smarsly BM (2015) Nitrogen-Doped Carbon Electrodes: Influence of Microstructure and Nitrogen Configuration on the Electrical Conductivity of Carbonized Polyacrylonitrile and Poly(ionic liquid) Blends. Macromol Chem Phys 216:1930–1944.
37. Amaral-Labat G, Szczurek A, Fierro V, Pizzi A, Celzard A (2013) Systematic studies of tannin-formaldehyde aerogels: preparation and properties. J Sci Technol Adv Mater 14:015001.
38. Thurner CW, Drexler X, Haug L, Winkler D, Kunze-Liebhäuser J, Bernardi J, Klötzer B, Penner S (2023) When copper is not enough: Advantages and drawbacks of using copper in de-NOx reactions over lanthanum manganite perovskite structures. Appl Catal B: Environ 331:122693.
39. Thurner CW, Bonmassar N, Winkler D, Haug L, Ploner K, Delir Kheyrollahi Nezhad P, Drexler X, Mohammadi A, van Aken PA, Kunze-Liebhäuser J, Niaei A, Bernardi J, Klötzer B, Penner S (2022) Who does the job? how copper can replace noble metals in sustainable catalysis by the formation of copper–mixed oxide interfaces. ACS Catal 12:7696–7708.
40. Ayiania M, Smith M, Hensley AJR, Scudiero L, McEwen J-S, Garcia-Perez M (2020) Deconvoluting the XPS spectra for nitrogen-doped chars: An analysis from first principles. Carbon 162:528–544.
41. Koopmann AK, Torres-Rodríguez J, Salihovic M, Schoiber J, Musso M, Fritz-Popovski G, Huesing N, Elsaesser MS (2021) Tannin-Based Nanoscale Carbon Spherogels as Electrodes for Electrochemical Applications. ACS Appl Nano Mater 4:14115–14125.
42. Saliger R, Fischer U, Herta C, Fricke J (1998) High surface area carbon aerogels for supercapacitors. J Non-Crystalline Solids 225:81–85.
43. Thommes M, Kaneko K, Neimark AV, Olivier JP, Rodriguez-Reinoso F, Rouquerol J, Sing KSW (2015) Physisorption of gases, with special reference to the evaluation of surface area and pore size distribution (IUPAC Technical Report). pac 87:1051–1069.
44. Amaral-Labat G, Munhoz MGC, Fonseca BCDS, Boss AFN, de Almeida-Mattos P, Braghiroli FL, Bouafif H, Koubaa A, Lenz e Silva GFB, Baldan MR (2021) Xerogel-like Materials from Sustainable Sources: Properties and Electrochemical Performances. Energies 14:7977.
45. Rasines G, Macías C, Haro M, Jagiello J, Ania CO (2015) Effects of CO2 activation of carbon aerogels leading to ultrahigh micro-meso porosity. Microporous Mesoporous Mater 209:18–22.
46. Guo S, Peng J, Li W, Yang K, Zhang L, Zhang S, Xia H (2009) Effects of CO2 activation on porous structures of coconut shell-based activated carbons. Appl Surf Sci 255:8443–8449.

47. Kröner J, Platzer D, Milow B, Schwan M (2024) Electrical conductivity of monolithic and powdered carbon aerogels and their composites. Mater Adv 5:8042–8052.
48. Wiener M, Reichenauer G, Hemberger F, Ebert HP (2006) Thermal Conductivity of Carbon Aerogels as a Function of Pyrolysis Temperature. Int J Thermophys 27:1826–1843.
49. Howaniec N (2019) Combined effect of pressure and carbon dioxide activation on porous structure of lignite chars. Materials 12:1326.
50. Roh J-S (2008) Structural study of the activated carbon fiber using laser Raman spectroscopy. Carbon Lett 9:127–130.
51. Liu G, Chen X, Ahmed SF, Ma W (2025) Urea assisted melamine N/O co-doping Activated carbon for high performance energy storage materials. J Power Sources 640:236652.
52. Celzard A, Marêché J, Payot F, Furdin G (2002) Electrical conductivity of carbonaceous powders. Carbon 40:2801–2815.
53. Wassner M, Eckardt M, Reyer A, Diemant T, Elsaesser MS, Behm RJ, Hüsing N (2020) Synthesis of amorphous and graphitized porous nitrogen-doped carbon spheres as oxygen reduction reaction catalysts. Beilstein J Nanotechnol 11:1–15.
54. Salihovic M, Zickler GA, Fritz-Popovski G, Ulbricht M, Paris O, Hüsing N, Presser V, Elsaesser MS (2019) Reversibly compressible and freestanding monolithic carbon spherogels. Carbon 153:189–195.
55. Kaniyoor A, Ramaprabhu S (2012) A Raman spectroscopic investigation of graphite oxide derived graphene, AIP Adv 2.
56. Lee MS, Whang DR, Song YH, Kim JT, Yang MH, Choi UH, Chang DW (2019) Effects of pyridine and pyrrole moieties on supercapacitive properties of imine-rich nitrogen-doped graphene. Carbon 152:915–923.
57. Fakhraei M, Mirzaei-Saatlo M, Asghari E (2024) A LiPF6 gel-polymer electrolyte for a solid-state supercapacitor with polyaniline/MnCo layered double hydroxide nanosheets as active electrode material. J Energy Storage 101:113930.
58. Karthikeyan A, Mariappan R, Bakkiyaraj R, Krishnamoorthy E (2023) High electrochemical performance of Co3O4-PVDF-NMP-based supercapacitor electrode. J Mater Sci: Mater Electron 34:728.
59. Barbieri O, Hahn M, Herzog A, Kötz R (2005) Capacitance limits of high surface area activated carbons for double layer capacitors. Carbon 43:1303–1310.
60. Lee MS, Choi H-J, Baek J-B, Chang DW (2017) Simple solution-based synthesis of pyridinic-rich nitrogen-doped graphene nanoplatelets for supercapacitors. Appl Energy 195:1071–1078.
61. Lv Y, Zhang L, Wei X, Qiu B, Zhang W, Qin Q, Jia D, He X, Liu Z, Wei F (2023) The emerging of zinc-ion hybrid supercapacitors: Advances, challenges, and future perspectives. Sustain Mater Technol 35:e00536.
62. Kraiwattanawong K, Tamon H, Praserthdam P (2011) Influence of solvent species used in solvent exchange for preparation of mesoporous carbon xerogels from resorcinol and formaldehyde via subcritical drying. Microporous Mesoporous Mater 138:8–16.
63. Turhan Kara I, Kiyak B, Colak Gunes N, Yucel S (2024) Life cycle assessment of aerogels: a critical review. J Sol-Gel Sci Technol 111:618–649.